7-7-2021

Optimization of load-bearing and impact energy absorption capacities of honeycomb structures by density gradation

Oyindamola Khadijat Rahman
Rowan University

www.manaraa.com

OPTIMIZATION OF LOAD-BEARING AND IMPACT ENERGY ABSORPTION CAPACITIES OF HONEYCOMB STRUCTURES BY DENSITY GRADATION

by

Oyindamola Rahman

A Thesis

Submitted to the
Department of Mechanical Engineering
Henry M. Rowan College of Engineering
In partial fulfillment of the requirement
For the degree of
Master of Science in Engineering
at
Rowan University
June 3, 2021

Thesis Chair: Behrad Koohbor, Ph.D.

Committee Members:
Chen Shen, Ph.D.
Nand Singh, Ph.D.

Acknowledgements

Foremost, I give thanks to Almighty God, for without his mercies and grace, this study would not have been possible. I would also like to appreciate my parents Mr. and Mrs. Rahman for their love, prayer, and sacrifices for educating and preparing me for the future.

Similarly, my deep and sincere gratitude goes to my esteemed research supervisor, Dr. Behrad Koohbor, for being the ideal advisor and for giving me the opportunity to do this research and providing invaluable guidance and insightful criticism which aided in the writing of this paper in numerable ways. Many thanks for his words of encouragement which have always been enlightening. I could not imagine a better advisor and it is a great privilege to study under his guidance.

I would like to thank my colleagues, Kazi, Jeeva, Robert and Nick whom I have worked with over the last two years for showing me support and giving me their time, energy, and expertise. The general help and friendship are greatly appreciated. Also, I express my gratitude to my little sisters, Oyinlola, Oyinkan, and Bolu for their support, prayers, and words of encouragement towards the actualization of this dream. May God continue to bless and keep them.

Last and certainly not the least, my express gratitude goes to Olayemi Shittu for going on this journey quite willingly with me. Thank you for always bolstering my spirits and for your unwavering believe in me and my abilities

Abstract

Oyindamola Rahman
OPTIMIZATION OF LOAD-BEARING AND IMPACT ENERGY ABSORPTION
CAPACITIES OF HONEYCOMB STRUCTURES BY DENSITY GRADATIONS
2020-2021
Behrad Koohbor, PhD.
Master of Science in Mechanical Engineering

Density gradation has been analytically and experimentally proven to enhance the load-bearing and energy absorption efficiency of cellular solids. This research focuses on the analytical optimization (by virtual experiments) of polymeric honeycomb structures made from flexible thermoplastics to achieve density-graded structures with desired mechanical properties. The global stress-strain curves of single-density honeycomb structures are used as input to an analytical model that enables the characterization of the constitutive response of density-graded hexagonal honeycombs with discrete and continuous gradations and for various gradients. The stress-strain outputs are used to calculate the specific energy absorption, efficiency, and ideality metrics for all density-graded structures. The analytical results are shown to be in good agreement with previous experimental measurements. The findings of this research suggest that the choice of an optimal gradient depends on the specific application and design criteria. For example, graded structures wherein low-density layers are dominant are shown to outperform high density uniform honeycombs in terms of specific energy absorption capacity while possessing higher strength compared with low density uniform structures.

iv

Table of Contents

List of Figures

List of Tables

Chapter 1

Introduction

Having high strength, an almost-flat collapse stress and a large densification strain are some of the promising mechanical properties of cellular materials that makes them applicable in energy-absorption applications [1]. Honeycomb structures (see Figure 1), one of the simplest cellular structure in nature has several favorable mechanical properties that has made it possible to be exploited in a variety of applications from biomechanics to automotive to aerospace [2-4] (Figure 2); its energy absorption properties have been useful as shock absorbers in the aerospace industries, it's load-bearing properties has been useful in packaging industries and it has also been found efficient in the biomedical industry as a replacement for prosthetics [5, 6].

Figure 1

Schematics of a Honeycomb Structure [7]
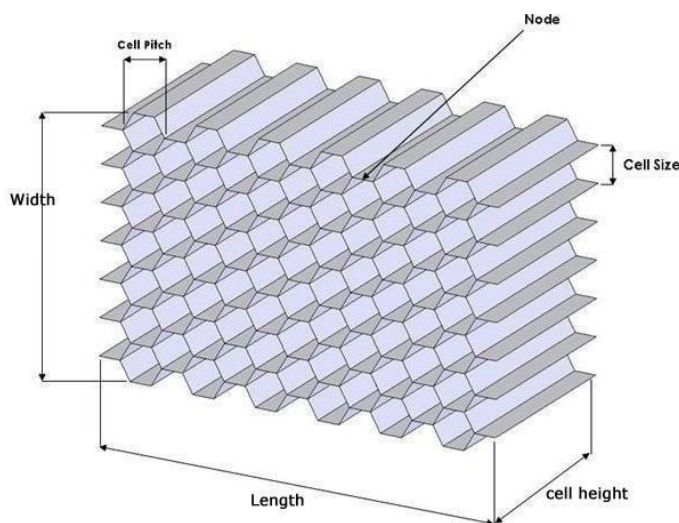
Figure 2

Honeycomb Crash Absorption Structure

Note. Made of injection molded thermoplastic polymer on a BMW i3 [8].

From literature, it has been proven that the density, mechanical characteristics, and the properties of honeycombs to absorb strain energy strongly depend on the cellular architecture and connectivity, as well as the ratio between their cell-wall thickness and cell-size [9-13] (Figure 3). Therefore, one of the most promising advantages of the use of honeycomb structures is the ability to tailor their mechanical and energy absorption performance simply by varying their cell shape, cell size, and cell-wall thickness. While increasing the cell-wall thickness in honeycombs is associated with an increase in their stiffness and strength, it can also lead to unfavorable properties such as higher structural weight and often lower energy absorption capacity [14, 15]. In contrast, the specific energy absorption (energy absorption normalized by density) of honeycombs can be enhanced by decreasing the cell-wall thickness, but at the cost of strength and stiffness

2

Figure 3

Mechanics of a Single-Density Honeycomb Structure
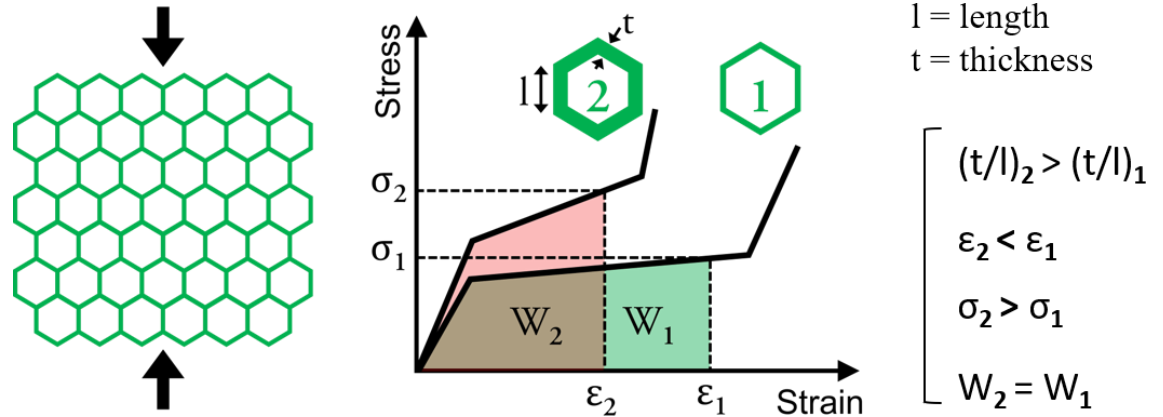
The concept of *density gradation* in cellular materials is derived from the juxtaposition between the dichotomy between stiffness/strength and energy absorption/density. The fundamental idea in density-graded cellular structures is to develop an integrated structure by spatially varying the local cell-wall thickness to cell-size ratio (equivalent to nominal density) which brings about the reduction in the overall weight of the structure while its load-bearing and energy absorption capacities are improved upon [16]. Previous studies suggest that density gradation can significantly improve the load-bearing, energy absorption, and damage resistance of density-graded foams [17-20]. The impact resistance of foams and other cellular structures were shown to improve remarkably by density gradation [21-23], these researchers have led to the development of helmets and other protective components with enhanced impact energy mitigating performance [24, 25].

3

With the rapid development of advanced manufacturing methods, engineers have more freedom in the design and manufacture of cellular structures and can create complex lattice structures or "Architected structures" [26-30]. 3D printing an additive manufacturing method provides the freedom to fabricate lattice structures with complex geometric designs that is unmatched by any other method [31-36]. Hexagonal honeycomb structures have been fabricated severally with 3D printing such as [36], which enables their fabrication with difference in cell wall thickness thereby resulting in varying nominal densities. This difference in densities affect the mechanical properties of the structures such as the weight, strength, energy absorption, etc. Additive manufacturing has given the opportunity for the optimization and improvement of these structures, thereby combining the favorable properties of structures with various densities to derive one optimized structure that is the best fit for a particular purpose. This optimization can be achieved by several ways; changing the geometry and topology of the cells [37], gradation of densities in one structure, development of multi-material structures [32], etc.

There has been extensive analytical, experimental, and theoretical work done on the in-plane and out-of-plane mechanical properties of honeycombs under static loading and dynamic crushing conditions for single density and graded density honeycombs. During the in-plane deformation of a honeycomb structure by compression [36, 38, 39], the cell walls first undergo bending which results in a linear elastic regime, thereafter followed by an almost linear plastic collapse at the collapse stress which shows presents itself depending on the properties of the material used (elastic buckling for elastomers, plastic hinging for plastics and brittle fracture for brittle materials). Finally, as the strain increases, opposite cell walls come in contact with each other, closing up the honeycomb

4

structure and leading to a sharp rise in the stiffness and the densification of the cell wall material [9].

For honeycomb structures with $t/l < 0.25$, Gibson and Ashby developed a mathematical model to derive a corresponding bi-linear stress-strain curve [7]. Zhang et al [39] computationally investigated the dynamic crushing behavior and energy absorption of honeycombs with density gradient. Ivanez et al [40] analyzed the crush behavior and energy absorption capability of aluminum honeycomb core using virtual compressive tests and varying the cell size and cell wall thickness and material. Mousanezhad *et al.* [41] investigated the effects of density gradation on in-plane dynamic crushing response and impact behavior of hexagonal honeycombs through computational modeling. Their modeling results indicated that density gradation can improve the impact response of hexagonal honeycomb structures. They also reported that variations in the gradient function significantly affects the crushing response of density-graded structures by altering the location of the failure localization sites and changing the plastic energy dissipation mechanisms. Bates *et al.* [36] performed experiments on the compressive behavior of 3D printed thermoplastic polyurethane (TPU) honeycombs with graded densities and discovered that graded hexagonal honeycombs structures.

have the ability to absorb the strain energy more effectively, but translates to lower efficiency in comparison with single-density structures. Galehdari et al [38] also conducted an analytical, experimental and numerical study of a graded honeycomb structure under in-plane impact load with low velocity. These researchers all show a consistent layer-by-layer deformation of the density-graded honeycombs. The layer with

5

the lowest density undergoes deformation and therefore densification first, followed by the next, etc., thereby resulting in a step-wise global stress-strain curve [36].

While there has been computational work done on honeycomb structures with density gradient and density gradation has been proved to be a good way to improve the energy absorption capabilities of cellular structures, there has been a lack of comprehensive computational work done on the optimization of a functionally graded honeycomb structure. This research takes advantage of both the honeycomb structure and advancement in manufacturing to produce a functionally graded honeycomb structure with the correct combination of densities that would give the best energy absorption, lightest weight and highest strength in just one architecture material. Using a MATLAB code, the local strain at each density layer is interpolated and the global strain corresponding to a particular stress is calculated. Further post work is done to derive the specific energy absorbed, ideality, etc. for different density gradients.

1.1 Motivation for Present Work

In recent years, density gradation has been proposed as a favorable approach that enables the development of lightweight, high strength, and high energy absorbing cellular solids. The basic idea behind the concept of density-graded cellular solids is to develop an integrated structure in which the local density is varied spatially and along certain directions such that the overall weight of the structure remains low while its strength and energy absorption capacity (as well as other properties, e.g., ductility, weight, etc.) are enhanced. Recent successes in the development of density-graded structures signals that density gradation can truly enhance the energy absorption of cellular solids, while also enabling the customization of the structural weight, load-bearing performance, and other

6

functionalities at the same time. Therefore, the interest in the design, fabrication, and mechanical characterization of density-graded cellular solids has witnessed a tremendous increase.

1.2 Objective of Thesis

The objective of this present work is to extend the previously proposed idea of gradient optimization into the area of graded honeycombs. To this goal, this work uses an analytical data-driven approach to determine the global stress-strain response of density-graded structures from the stress-strain response of their single-density constituents. The proposed analytical approach facilitates *virtual testing* of dozens of density-graded honeycombs via a computational cost saving methodology that can be an efficient alternative to finite element modeling. The proposed approach uses a data-driven algorithm that facilitates the characterization of the load-bearing and energy absorption performance of density-graded honeycombs, thereby enabling the identification of optimal gradients. Specifically, the approach presented in this work provides a practical solution to the design of honeycombs with high energy absorption and strength properties.

1.3 Outline of Thesis

The information proceeds as follows: **Chapter 2** describes the background and justification of the proposed idea. Model development and various gradients examined are discussed in **Chapter 3**. In **Chapter 4**, the validity of the modeling approach is discussed first. Detailed analysis of 3-stage and continuously graded honeycombs are then elaborated. The potential applicability of the presented approach in the design and development of novel ordered cellular structures with superior strength and energy

7

absorption characteristics as well as suggested recommendations are highlighted in

Chapter 5.

Chapter 2

Density-Dependent Constitutive Model

During the in-plane deformation of a honeycomb structure by compression, cell walls first undergo bending which results in a linear elastic regime, thereafter followed by an almost linear plastic collapse at the collapse stress which presents itself in the form of a plateau in the stress-strain curve, depending on the properties of the material used (elastic buckling for elastomers, plastic hinging for plastics and brittle fracture for brittle materials). Finally, as the strain increases, opposite cell walls come in contact with one another, closing up the honeycomb structure and leading to a sharp rise in the stiffness. The latter phenomenon marks the onset of the densification stage [9]. For honeycomb structures with $t/l < 0.25$ (with t and l denoting cell wall thickness and cell edge size, respectively), Gibson and Ashby developed a mathematical model to derive a corresponding bi-linear stress-strain curve [9]

For hexagonal honeycomb structures with a small t/l ratio, loaded in the in-plane direction, the effect of axial and shear deformation on each hexagonal cell are negligible compared to that of the bending of the cell walls [9]. Using the Gibson and Ashby equations, the density-dependent stress-strain data for each honeycomb structure was calculated. For uniform hexagonal honeycombs with cell-wall thickness t and cell edge length l (**Figure 4a**), regular cells; $h=l$ and $\theta=30^0$ and are isotropic

The relative density, *i.e.*, the density of the honeycomb divided by the density of the cell-wall material, is given as [9];

$$\frac{\rho^*}{\rho_S} = \frac{2t}{\sqrt{3}\,l} \tag{1}$$

where ρ^* is the density of the hexagonal honeycomb structure and ρ_S is the density of the base material.

Elastic modulus in tension and compression can be assumed as the same and is given as [9];

$$\frac{E_1^*}{E_S} = \frac{E^*}{E_S} = 2.3\left(\frac{t}{l}\right)^3 \tag{2}$$

Where E_1^* (elastic modulus of the honeycomb structure in the X_1 direction) = E_2^*(elastic modulus of the honeycomb structure in the X_2 direction) because the honeycomb is made up of regular and isotropic hexagons.

For honeycombs fabricated from elastic-perfectly plastic parent material which undergo plastic hinging, the plastic collapse stress (σ_{pl}^*) is expressed as [9];

$$\frac{\sigma_{pl}^*}{\sigma_{ys}} = \frac{2}{3}\left(\frac{t}{l}\right)^2 \tag{3}$$

where σ_{ys} is the yield stress of the cell wall material. The corresponding plastic collapse strain (ε) is given as [9];

$$\varepsilon = \frac{\sigma_{pl}^*}{E^*} \tag{4}$$

After the cell walls have collapsed and all pore space has been squeezed out, the densification strain (ε_D) of an ideal and isotropic honeycomb structure is expressed as [9];

$$\varepsilon_D = 1 - 1.616 \frac{t}{l}$$

(5)

It has been discovered that there are two factors that contribute to the strain hardening of cellular materials; the strain hardening of the cell wall material and the geometric hardening due to strut reorientation. Mangipudi *et al*. [42] derived a density-dependent relation between the hardening tangent modulus of the material (H') with that of a regular hexagonal honeycomb structure (H_S) which is given by;

$$\frac{H'}{H_S} = \frac{4}{\sqrt{3}} \left(\frac{t}{l}\right)^3$$

(6)

The combination of both the density-dependent bi-linear proposed by Gibson and Ashby [7] and that of the strain hardening proposed by Mangipudi *et al*. [42] produces a tri-linear stress-strain curve for a regular hexagonal honeycomb structure that is similar to those obtained experimentally.

Note that the densification strain in cellular solids is also equivalent to a strain value that corresponds with maximum efficiency (see **Eq. 8**) [43, 44]. **Eqs. 2-5** allow one to construct bi-linear stress-strain curves that describe the global response of elastomeric hexagonal honeycombs under in-plane compression. These bi-linear constitutive curves can be used to estimate the energy absorption capacity of the honeycomb in response to compressive stress. The energy absorption metrics, namely the absorbed strain energy (E_s) and efficiency (η), can be determined as [43]:

11

$$E_s(\varepsilon) = \int_0^\varepsilon \sigma(\varepsilon)d\varepsilon \tag{7}$$

$$\eta(\varepsilon) = \frac{\int_0^\varepsilon \sigma(\varepsilon).d\varepsilon}{\sigma} \tag{8}$$

Considering the density-dependent constitutive and energy absorption relations described above, it is reasonable to assume that the energy absorption of a hexagonal honeycomb is directly proportional to $(t/l)^3$, as the energy is a product of stress and strain. Similarly, the specific energy and specific efficiency, i.e. energy absorption and efficiency metrics normalized by density, will be proportional to $(t/l)^2$ and $(t/l)^{-1}$, respectively. Finally, as indicated by **Eq. 5**, the strain range over which a hexagonal honeycomb retains its energy absorption efficiency decreases linearly with (t/l) [44].

Figure 4

Schematic of a Single Elastomeric Hexagonal Cell
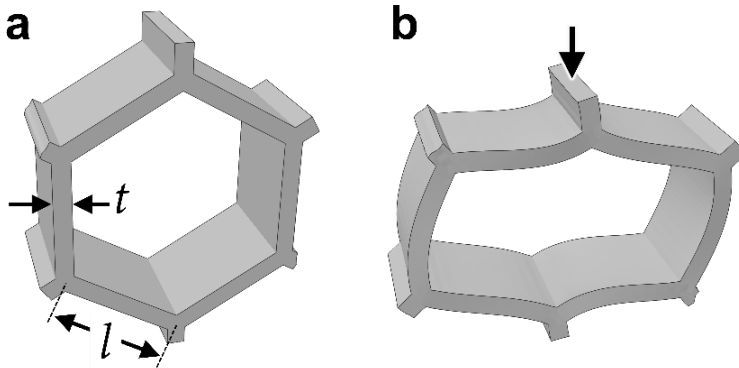
Note. (a) undeformed, and (b) deformed states

The interdependence of density, strength, and energy absorption capacity in hexagonal honeycombs implies that, from a design perspective, there is not a single density that simultaneously offers both high strength and excellent energy absorption performance at a low mass. This statement is graphically shown in **Figure 5** wherein bi-linear stress-strain and specific energy absorption curves are constructed for elastomeric hexagonal honeycombs with t/l ratios ranging from 0.1 to 0.25. To construct these curves, we have considered thermoplastic polyurethane (TPU) with density, Young's modulus, and strain hardening modulus of 1235 kg/m^3, 21.2 MPa, and 1.50 MPa, respectively, extracted from [14, 45]. Stress-strain and energy-strain curves shown in **Figure 5** confirm that strength and energy absorption performance of elastomeric hexagonal honeycombs are strongly dependent on the relative density of the structure, while the latter is also a function of the compressive strain. For example, according to the data shown in **Figure 5b**, designing of a hexagonal component with a 25 J/kg energy absorption capacity can be achieved through the use of several t/l ratios, but at the cost of strength and/or overall deformability of the structure.

The interplay between density-dependent strength and energy absorption performance of hexagonal honeycombs suggests that it is possible to benefit from the design of honeycombs with a *spatially-variable* density in order to optimize the strength-energy absorption capacity of the structure while maintaining a low overall density. In the forthcoming sections, we elaborate on our approach to achieving this goal.

While the simplified approach discussed here to explicate the density-dependent behavior of hexagonal honeycombs is valid for t/l ratios lower than 0.25 [9] and we recognize that the structures examined in the next section and throughout the remainder

13

of this article have *t/l* ratios higher than 0.25, the trends discussed in this section were

shown to remain valid for larger *t/l* ratios, as well [14].

Figure 5

Stress-Strain-Specific Energy Absorption Metrics
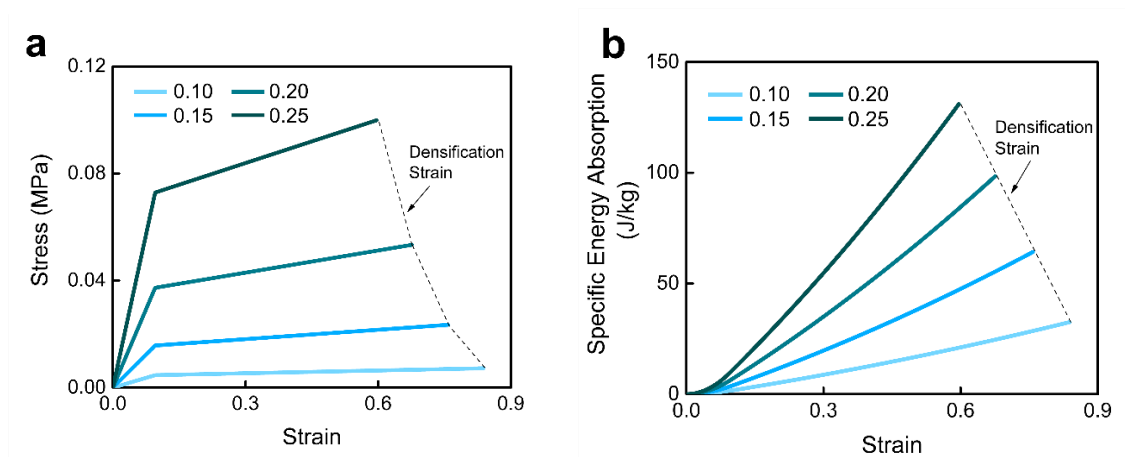
Note. Variation of (a) Compressive Stress and (b) Specific Energy Absorption, with respect to compressive strain for hexagonal honeycomb structures with t/l ratios ranged from 0.10 to 0.25. The dashed lines mark the locus of densification strains.

Chapter 3

Modeling

3.1. Materials and Gradients

Hyperplastic hexagonal honeycomb structures manufactured by Bates *et al.* [36] with various nominal densities were considered as input to our model. These honeycomb structures were fabricated by Bates *et al*. [36] from thermoplastic polyurethane (TPU) via fused filament 3D printing and in three relative densities of $\rho^* = 0.26$, 0.37, and 0.5. Global stress-strain data associated with these structures were digitized from the data published in [36]. 3-stage graded hexagonal structures with a total number of 9 rows (see **Figure 6a**) and with various gradients were studied. 28 different gradients with details listed in **Table 1** were studied. These 28 gradient combinations cover the range of structures with the highest relative density (case No. 1, [1:1:7]) to the lowest relative density (case No. 28, [7:1:1]), and includes the linear 3-stage gradient (case No. 16 [3:3:3]). The latter gradient is also used for the validation of the modeling results with the experimental measurements reported by Bates *et al*. [36]. For each gradient, the nominal relative density of the structure was calculated as:

$$\rho^* = \frac{\sum_{i}^{3} \rho_i^* t}{\sum_{i}^{3} t_i} \tag{9}$$

where, ρ_i^* and t_i are the relative density and the corresponding number of layers (see **Table 1**). The total number of rows (*i.e.,* 9) was selected to resemble the structures studied by Bates *et al*. [36].

15

The approach presented here is independent of the architecture, cell geometry, and the material used in the fabrication of a honeycomb structure. The only limitations associated with the application of the present modeling approach are that the structures must ideally have zero Poisson's ratios and the loading rate is limited to slow quasi-static conditions, *i.e.* the strain rate sensitivity of the material is not implemented in the current model.

Table 1

Gradients and Properties of Hexagonal Honeycombs

Case Number	No. of LD Layers (t_1) †	No. of MD Layers (t_2)	No. of HD Layers (t_3)	Relative density of
1	1	1	7	0.459
2	1	2	6	0.444
3	1	3	5	0.430
4	1	4	4	0.416
5	1	5	3	0.401
6	1	6	2	0.387
7	1	7	1	0.372
8	2	1	6	0.432
9	2	2	5	0.418
10	2	3	4	0.403
11	2	4	3	0.389
12	2	5	2	0.374
13	2	6	1	0.360
14	3	1	5	0.406
15	3	2	4	0.391
16	3	3	3	0.377
17	3	4	2	0.362
18	3	5	1	0.348
19	4	1	4	0.379
20	4	2	3	0.364

Case Number	No. of LD Layers (t_1) †	No. of MD Layers (t_2)	No. of HD Layers (t_3)	Relative density of
21	4	3	2	0.350
22	4	4	1	0.336
23	5	1	3	0.352
24	5	2	2	0.338
25	5	3	1	0.323
26	6	1	2	0.326
27	6	2	1	0.311
28	7	1	1	0.299

Note. LD: Low Density (ρ_1^* =0.26), MD: Medium Density (ρ_2^* =0.37), HD: High Density

(ρ_3^* =0.50)

In addition to the 28 three-stage graded structures, three cases of *continuous gradations* were also examined. The continuously graded structures in this work were designed based on a previous study performed on density-graded polyurethane foams [18]. Details regarding the cell configuration and spatial distribution of local relative density in the examined continuously- graded structures are shown in **Figure 6b** and **Table 2**, respectively. The three continuous gradient cases investigated in this work, namely, linear, concave, and convex, resemble the continuous gradients with gradient exponents of 1, 5, and 0.2, respectively, studied in [18]. In all continuous gradient cases, the relative density of the 1st and the 9th layer were kept constant and at 0.26 and 0.5, respectively. Depending on the gradient type (linear, convex, or concave), appropriate densities were assigned to layers numbered 2 to 8. The constitutive responses of these middle layers were obtained by an interpolating operator applied to the digitized stress-strain data of single-density structures with $\rho^* = 0.26$, 0.37, and 0.5. Nominal relative densities for the

17

continuously-graded structures were calculated using **Eq. 9.** As will be discussed in the

next section, due to the one-dimensional nature of the proposed model, the number of

cells in the horizontal direction is not considered.

Figure 6

Schematic of Density-Graded Honey Comb Structures
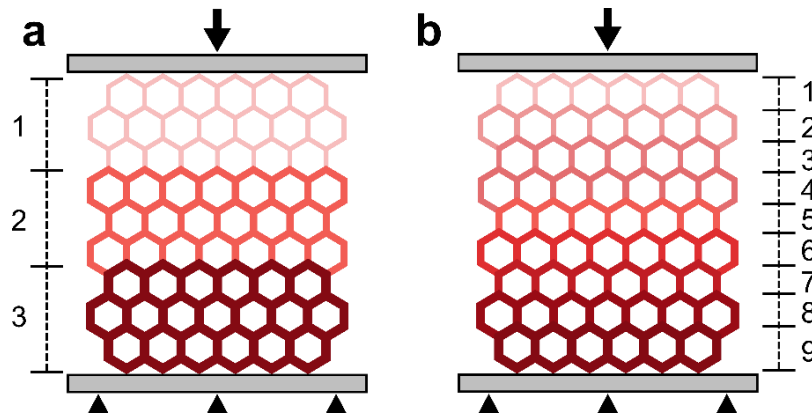
Note. Schematic of (a) 3-stage graded and (b) continuously graded structures examined in
this work. Both schematics show gradients with a linear increase in density. Different
colors are indicative of different densities.

Table 2

Continuously Graded Honeycombs

Layer No.	Gradient		
	Linear	Convex	Concave
1	0.26	0.26	0.26
2	0.29	0.42	0.26
3	0.32	0.44	0.26
4	0.35	0.46	0.26
5	0.38	0.47	0.27

18

Layer No.	Linear	Convex	Concave
6	0.41	0.48	0.28
7	0.44	0.49	0.32
8	0.47	0.50	0.38
9	0.50	0.50	0.50
Relative density of structure (ρ^*)	0.38	0.45	0.31

Note. Gradients and properties of continuously graded honeycombs examined in this work

3.2. Analytical Model Development

To derive the global stress-strain data for a density graded honeycomb structure, there is no straightforward method. However, it can be calculated by the method of inversely calculating the global stress value from known local stress values. In the case of density-graded honeycombs, the local density is predetermined by a known distribution function, herein referred to as the *gradient*. Besides, the assumption of a uniaxially applied stress also leads to a spatially constant local stress, given that the body forces are negligible and that the global force (stress) is applied quasi-statically, *i.e.* no acceleration [46, 47]. In such conditions, the local axial stress applied at any given location along the axis of the structure will be equal to the stress applied globally on the structure. The known density-stress pair can then be used as input to an analytical model that outputs the local strain at the location of interest. The process of inversely calculating the local strain is as follows:

1. The stress-strain data of the single-density honeycomb structures are used to

19

generate a stress-strain-density dataset. The desired gradient is also used as another input, wherein the local density is known at any given location (y) along the honeycomb axis.

2. A virtual global stress is applied incrementally. At a location with known density and for a given global stress increment, assuming equivalence between global and local stress, the corresponding local strain is calculated using a scattered data interpolation process applied to the stress-strain-density dataset. The interpolation process in this work is performed using a triangulation-based natural neighbor interpolation method with C^1 continuity.

3. Repeat *Step 2* for all layers along the axis of the honeycomb structure until all local strains corresponding with the global stress increment are obtained. Global strain corresponding with the global stress increment is calculated by integrating local strains along the *y*-axis.

4. Update the global stress increment and repeat *Step 2* and *Step 3* until the full global stress-strain response of the given gradient is obtained. Repeat the above process for all gradients.

Once all global constitutive data are obtained, the energy absorption metrics, namely the absorbed energy (E_s), efficiency (η), and ideality (I) can be determined using **Eqs. 6**, **7**, and **9**, respectively [48].

$$I(\varepsilon) = \frac{\int_0^\varepsilon \sigma(\varepsilon).d\varepsilon}{\sigma\varepsilon} \tag{9}$$

where, σ and ε denote global stress and global strain, respectively. For all cases studied

20

in this work, the maximum global stress applied to the graded structures was 2 MPa. The global stress was applied in increments of 0.01 MPa. Also, considering the rate-independent nature of the work, strain rate and its effects on the load-bearing and energy absorption performance was not considered. For single-density structures, the densification strain (ε_d) was evaluated as the strain at which the efficiency parameter (η) is maximum [49]. For 3-stage graded structures, the efficiency curves will have three peaks corresponding to the three distinct density regions within the structures. In such cases, the strain associated with the last local peak is considered as the nominal densification strain of the structure. The same approach is applied to continuously graded structures, wherein the nominal densification strain of the structure is identified as the global strain corresponding with the last local peak in the efficiency curve.

The data-driven model described above can be applied to any gradient function as long as the basic assumptions (*i.e.* quasi-static and uniaxial stress state) are satisfied. The analytical model used in this work was scripted in MATLAB. Obtaining the complete output dataset that contained the global stress-strain and energy absorption data of all 28 gradients listed in **Table 1** took approximately 40 minutes using a personal computer with 2.4 GHz processor and 8 GB of memory.

21

Chapter 4

Model Validation

4.1. Model Validation and Deformation Mechanism

The accuracy of the model predictions in this work was validated through reproducing the results obtained by Bates *et al*. [36] for 2-stage and 3-stage graded structures. For brevity, results of the 2-stage gradations are provided as **Supplemental Information**. **Figure 4** shows the comparison between the model predictions obtained from the data-driven model proposed in this work and the experimental measurements reported in Bates *et al*. [36]. Results shown in this figure include the stress-strain, specific energy, and efficiency data for a 3-stage gradient with a linear density distribution, i.e. each density constitutes 3 out of 9 layers of the structure (case No. 16 in **Table 1**). The model predicted data and experimental measurements show almost identical results, confirming the validity of the modeling efforts in this work.

The stress-strain curve obtained for the 3-stage graded structure shows a step-wise trend with three distinct yielding and plateau regions. This behavior has also been observed for graded foams [18] and functionally graded lattice structures [50, 51] and originates from the consecutive yielding and densification of the individual single-density regions in the structure. Upon the application of a compressive uniaxial load on a density-graded structure, such as the one studied here, all single-density regions undergo linear deformation first, while the larger portion of the deformation is exerted in the lowest density region. The linear deformation condition maintains until the global stress reaches the yield strength of the lowest-density layer yields. This so-called yield strength depends

22

on the mechanical nature of the material that constitutes the cell-walls, as well as the size,shape, and geometry of the cells [9]. Considering the elastomeric behavior of the base polymer studied in this work (i.e., TPU), the yielding of the honeycomb structure is governed by the elastic instability of cells, as also characterized by in-situ observations reported in Bates et al. [36]. Regardless, the collapse of cells in the lowest density region is manifested by the first step-wise increase in the stress-strain response of the 3-stage structure. By further increasing the compressive load, the lowest density layer deforms nonlinearly, while the other two layers remain in their linear deformation regime. When the global stress reaches the yield stress of the second lowest density region, the same mechanism takes place and the second step is formed on the stress-strain curve. These successive layer-wise collapses and deformation mode transitions continue until all density regions yield. Further increase of the load will result in the full densification of the entire structure (also initiated from the lowest density region), shown by a steep increase in the stress-strain response.

Densification strains for the three single-density structures as well as the 3-stage graded honeycomb are marked on the graphs in **Figure 7a**. The nominal densification of the 3-stage graded structure is shown to be higher than that of all single-density constituents. This observation is consistent with those made by Maskery *et al*. [50] on density-graded lattices 3D fabricated from polyamide PA2200, which indicates the superior energy absorbing properties of density graded structures compared with their uniform density equivalent structures. To further examine the energy absorption performance of graded vs. single-density structures, specific energy and efficiency responses were determined and compared in **Figure 7c,d** and **Figure 7e,f**, respectively. The specific energy curves plotted for single density structures show a single shoulder point, whereas the graded structures show multiple shoulder points, corresponding to the

23

number of density regions in the structure. The shoulder points in all cases also correspond to the points of maximum efficiency, as shown in Figure 7e,f. The enhanced energy absorption of a graded structure over an equivalent uniform structure is revealed in comparing the specific energy curves obtained for the 3-stage structure with the single-density structure with relative density $\rho^* = 0.37$. Despite the <2% difference in their nominal density, the graded structure shows higher amounts of energy absorption over an extended stress range. Specifically, except for a narrow stress range of *ca*. 0.15-0.6 MPa, the graded structure outperforms the single-density structure in terms of the amount of energy absorbed by an average of ~10%. On the other hand, comparing the efficiency curves of the two structures reveals that while the overall energy absorbing capacity of the 3-stage graded honeycomb is slightly better than that of the single-density structure, the efficiency response of the former is still inferior to that of the latter. Although this observation implicitly points to the enhanced strength of the graded structure, it also raises the question about the performance of the other 27 cases in terms of combined strength and energy absorption characteristics.

Figure 7

Stress-Strain, Specific Energy, and Efficiency Diagrams [34]
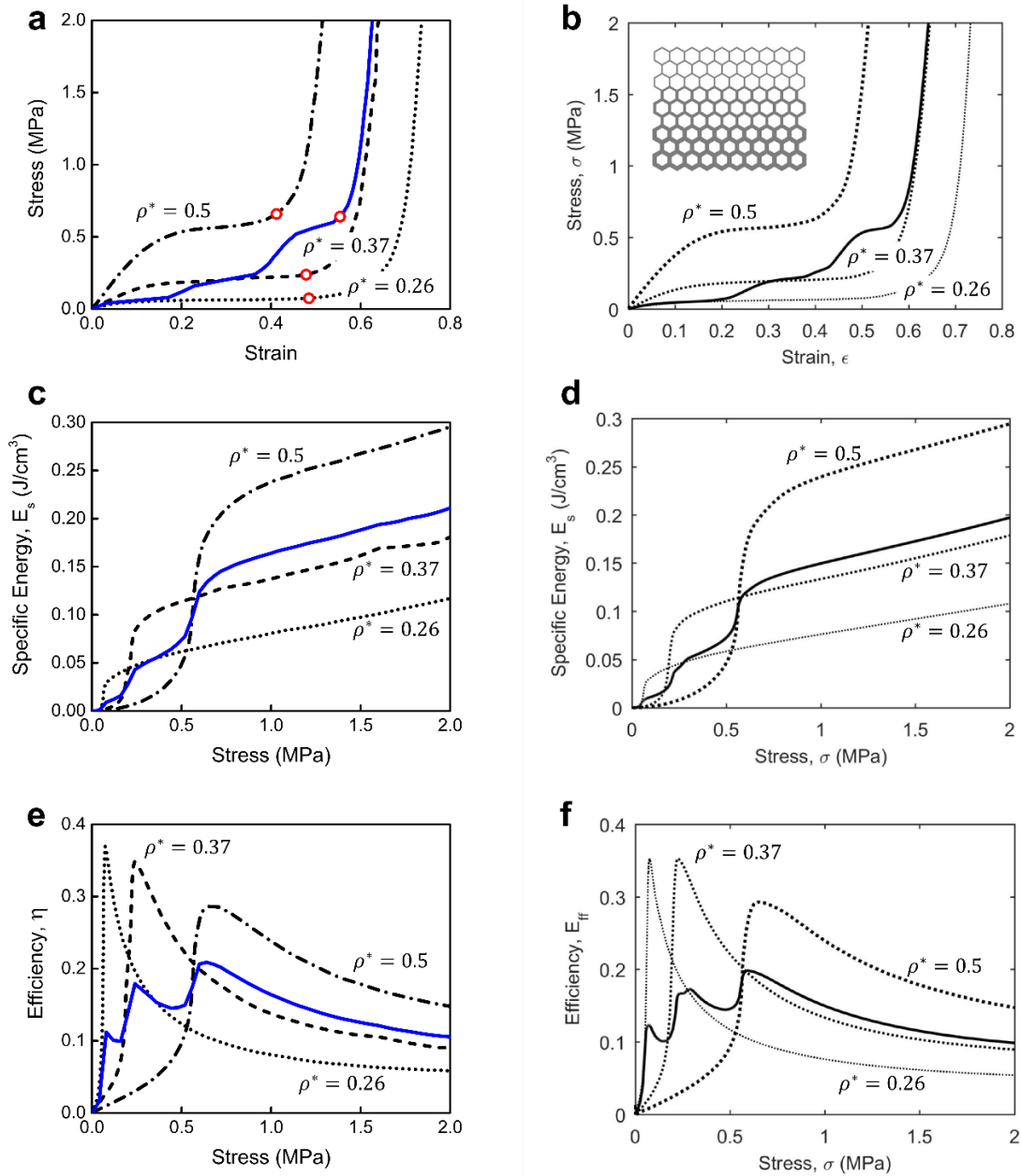
Note. single-density and 3-stage graded hexagonal honeycomb ($\rho^* = 0.377$) obtained from model (a,c,e) and experiment (b,d,f). dashed and dotted lines represent the single-density structures. Solid lines denote the variable of interest for the 3-stage graded structure. The hollow red circles in (a) mark the densification strains. The experimental data in panels (b) , (d), and (f) are

4.2. Strength-Energy Absorption Correlation

Stress-strain responses of a subset of the 28 three-stage cases examined in this work are shown in **Figure 8a**. The subset shown in this figure includes all cases wherein the middle-density layer makes only 1 out of 9 layers in the structure (see **Table 1**). The stress-strain curves shown include that of case No. 1 [1:1:7], i.e. the structure with the highest nominal density, as well case No. 28 [7:1:1], i.e. the one with the lowest nominal density. The step-wise stress-strain pattern is observed for all cases in **Figure 8a**, suggesting that the general deformation mechanism explained earlier in **Section 4.1.** is independent of gradient. Nevertheless, the extent of the stress plateaus and, more importantly, the nominal densification strains (**Figure 8b**) are found to be strongly dependent on the gradient.

Figure 8b shows densification strains for single-density and 3-stage graded structures. The single-density structures in this figure are marked as LD, MD, and HD, corresponding with low ($\rho^* = 0.26$), medium ($\rho^* = 0.37$), and high density ($\rho^* = 0.5$) structures, respectively. With the exception of a few cases (case No. 1, 2, 8) density-grade structures show significantly higher densification strains compared with all single-density honeycombs.

26

Figure 8

Strain Relationship Metrics
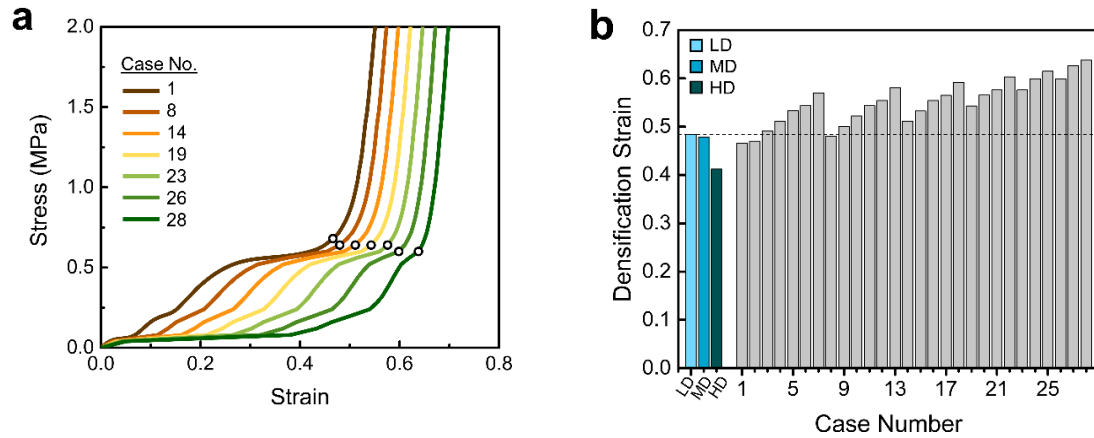
Note. Stress-strain curves for a subset of 3-stage graded structures, ranged from the lowest density to highest density cases. Densification strain is marked on each curve with a hollow circle. (b) A comparison between the densification strains of single-density and all 3-stage gradients examined in this work. The horizontal dashed line marks the highest densification strain in the single-density structures

Energy absorption metrics for a representative subset of the 3-stage graded structures are shown in **Figure 9**. Specific energy trends in **Figure 9a** resemble those shown earlier in **Figure 7c**, i.e. curves with three shoulder points. Higher density gradients (represented by lower case numbers) show a higher energy absorption performance among the subset of cases show in **Figure 9a**. The amount of energy absorbed by all 3-stage graded structures at their densification strains was determined and normalized by the corresponding density of each structure. The results are presented in **Figure 9b** as another indicator of the effectiveness of gradation in enhancing the overall energy absorption capacity. A great majority of 3-stage graded structures show slightly lower specific energy at densification strain compared with the HD single-density honeycomb. Interestingly, all 3-stage graded structures, regardless of their gradient, show

27

approximately 30% improvement in the same metric compared with the MD single-density honeycomb, and about 200% improvement compared with the LD single-density honeycomb.

Efficiency and ideality metrics for the same subset of cases are shown in **Figure 9c** and **Figure 9d**, respectively. All curves shown in these figures indicate a three-peaked pattern that corresponds with the number of density regions in the structure. A comparison between the efficiency and ideality curves for different cases shows that the intensity of the third peak increases for lower case numbers. This behavior stems from the increased contribution of the HD layer in gradients with lower case numbers.

Figure 9

Specific Energy Absorption Correlation
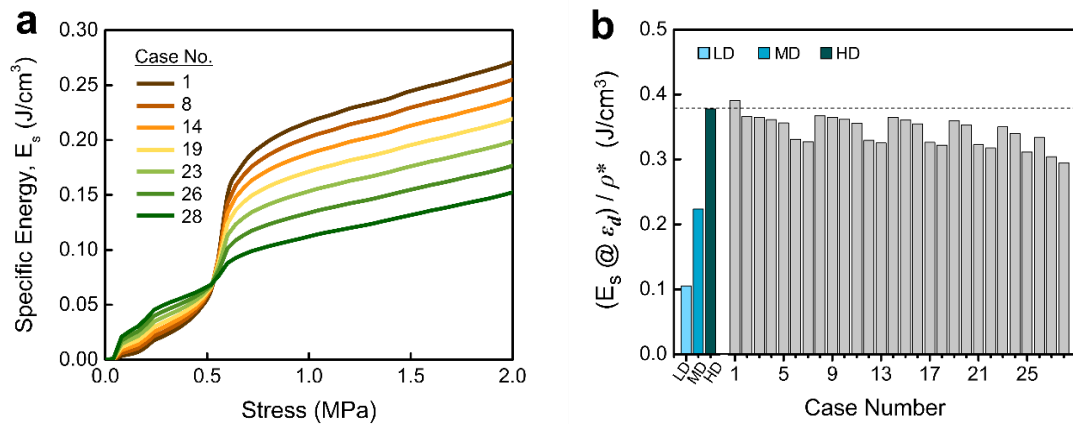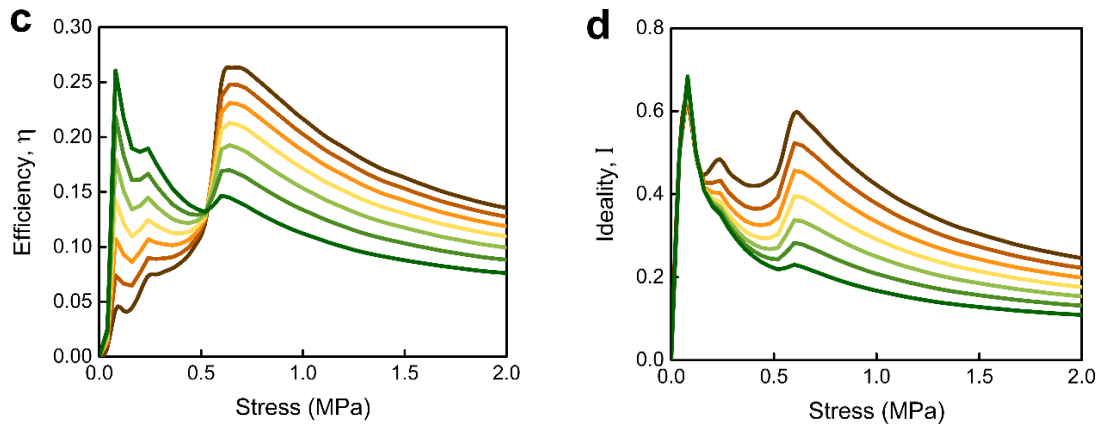
Note. Variation of specific energy as a function of stress for a subset of 3-stage graded structures, ranged from the lowest density to highest density cases. (b) Energy absorbed at the point of densification normalized by the density, $\left(E_s @ \varepsilon_d \right) \big/ \rho_*$, plotted for all single-density and 3-stage graded structures. Efficiency-stress and ideality-stress curves for the same subset are shown in (c) and (d), respectively.

It is documented that cellular solids show their highest energy absorption capacity over a strain range that is bound by those corresponding to maximum ideality and maximum efficiency, the latter being indicative of the densification strain, as well [48]. These two critical strains were identified for all cases listed in **Table 1**, and the strain range bound between the two critical strains were determined and plotted in **Figure 10**. The lower and upper bounds on the individual columns in **Figure 10** are associated with the strain at maximum ideality and densification points, respectively. In general, higher case numbers which associate with lower density gradients show a smaller strain range. Also, the last case number in every batch, which marks the gradients with the largest portion of MD constituents, outperforms other gradients in the batch. Accordingly, case No. 7 shows the highest strain range among all other gradients. To better realize the response of this particular gradient, we have plotted the stress-strain and energy response of case No. 7 in **Figure 11**. The stress-strain response of this gradient is close to that of

29

the MD structure, except two slight variations at the beginning and the end of the plateau region. Besides, the relative density of case No. 7 is also very close to that of the MD structure, with a difference of <1%. Despite such negligible differences, the graded structure is found to have at least 17% higher densification strain compared with all single-density structures. The energy absorption of the graded structure is also shown to be at least 6% higher than that of the MD structure at stress levels above 0.6 MPa.

Figure 10

Strain Range
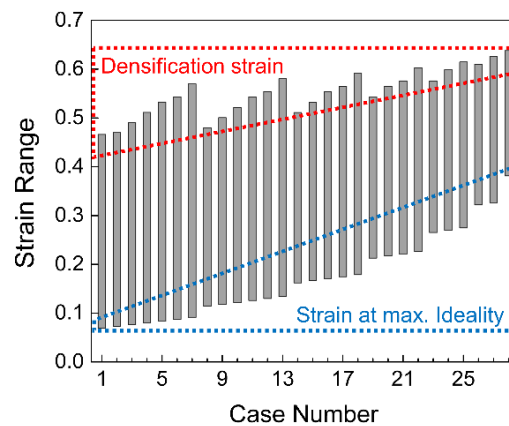
Note. Strain range bound by those corresponding with maximum ideality and densification for the 28 cases of 3-stage graded structures.

Figure 11

Stress-Strain and Specific Energy-Stress Responses
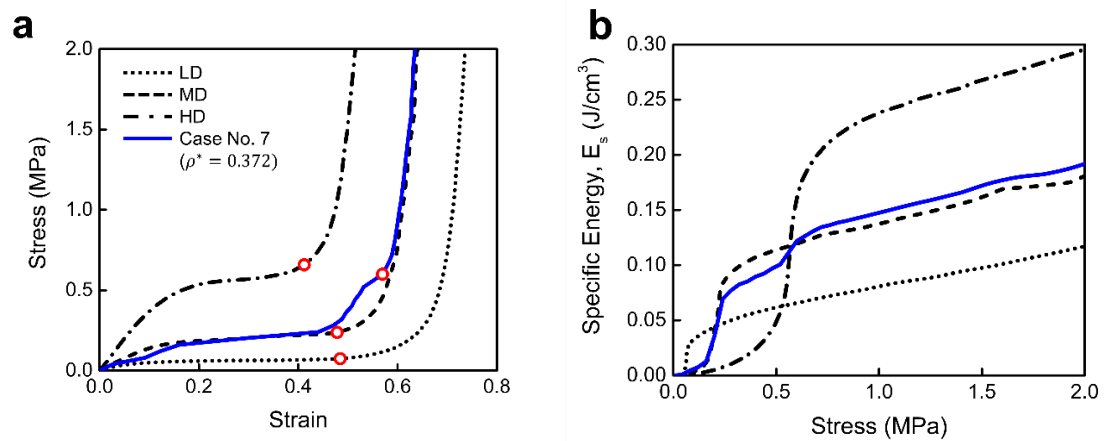
Note. Comparing the (a) Stress-Strain and (b) Specific Energy-Stress responses single-density structures with those of the 3-stage graded structure with [1:7:1] gradient (case No. 7).

4.3. Hexagonal Honeycombs with Continuous Gradients

Consistent with previous studies [36], results presented and discussed in the previous section showed that 3-stage density-graded honeycomb structure can potentially outperform their single-density counterparts in terms of combined strength and energy absorption capacity. Previous observations made on similar structures [48] as well as on rigid foams [18] had confirmed that the performance of density-graded structures can be further enhanced by continuous gradation. The concept of continuous gradation was implemented in this work through the study of three different cases, namely linear, convex, and concave gradients. The distribution of relative density in these three structures is shown in **Figure 12**. The nominal relative density of the three gradients are provided in **Table 2**.

31

Figure 12

Distribution of Relative Density
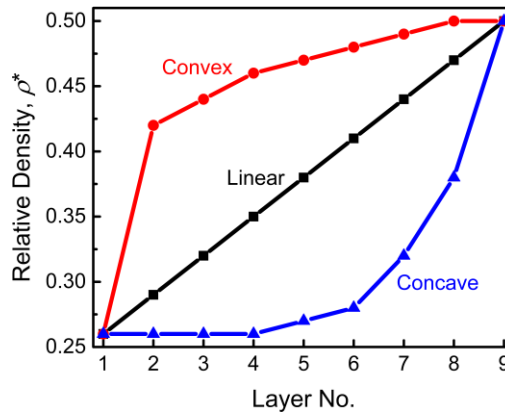
Note. Distribution of relative density in continuously graded structures with linear, concave, and convex gradients.

An approach similar to that applied to the 3-stage graded structures was used to evaluate the strength and energy absorption behaviors of the three continuously graded structures. **Figure 13** shows the stress-strain and the corresponding energy metric curves (specific energy, efficiency, and ideality) for the three continuously graded structures. Curves for single-density honeycombs are also shown for comparison. The general shape of the stress-strain curves if different for the continuously graded honeycombs compared with the 3-stage structures. Although the same step-wise yielding and densification mechanisms are still valid for continuously graded structures, the higher number of steps, which is directly correlated with the higher number of densities, masks the distinct steps on the stress-strain curves, especially for the linear gradient (see **Figure 13a**). Both linear and convex gradients show higher strength than the concave gradient as well as the LD and MD honeycombs. This observation is particularly important for the linear

32

gradient whose density is close to that of both the MD honeycomb (see **Table 2**) and the 3-stage discretely graded structure (see **Figure 7a**) but shows a noticeably higher strength at strains >0.2. From an energy absorption perspective, linear and convex gradients show an enhanced energy absorption capability compared with LD and MD honeycombs as well as concave gradient at stresses >0.5 MPa. On the other hand, the strain energy absorbed by the concave gradient outperforms those of linear and convex gradients as well as the HD honeycomb at stresses <0.4 MPa.

The strength-energy absorption dichotomy also reveals itself in efficiency and ideality data obtained for the continuously graded structures. The efficiency responses of the continuously graded honeycombs show significant differences in terms of their general shape and value. For example, while the concave gradient indicates a lower maximum efficiency than all other cases, it retains its high efficiency over a wider stress range. In contrast, both linear and convex gradients show single efficiency peaks at higher stress values but with steeply decaying values after reaching their relative efficiency peaks. The ideality curves also show quite different patterns, wherein the convex gradient indicates a distinct double-peak curve, with higher ideality values over a wide range of stresses while the other two continuous gradients (linear and concave) show a single peak at low stress levels.

Figure 13

Continuously Graded Structures
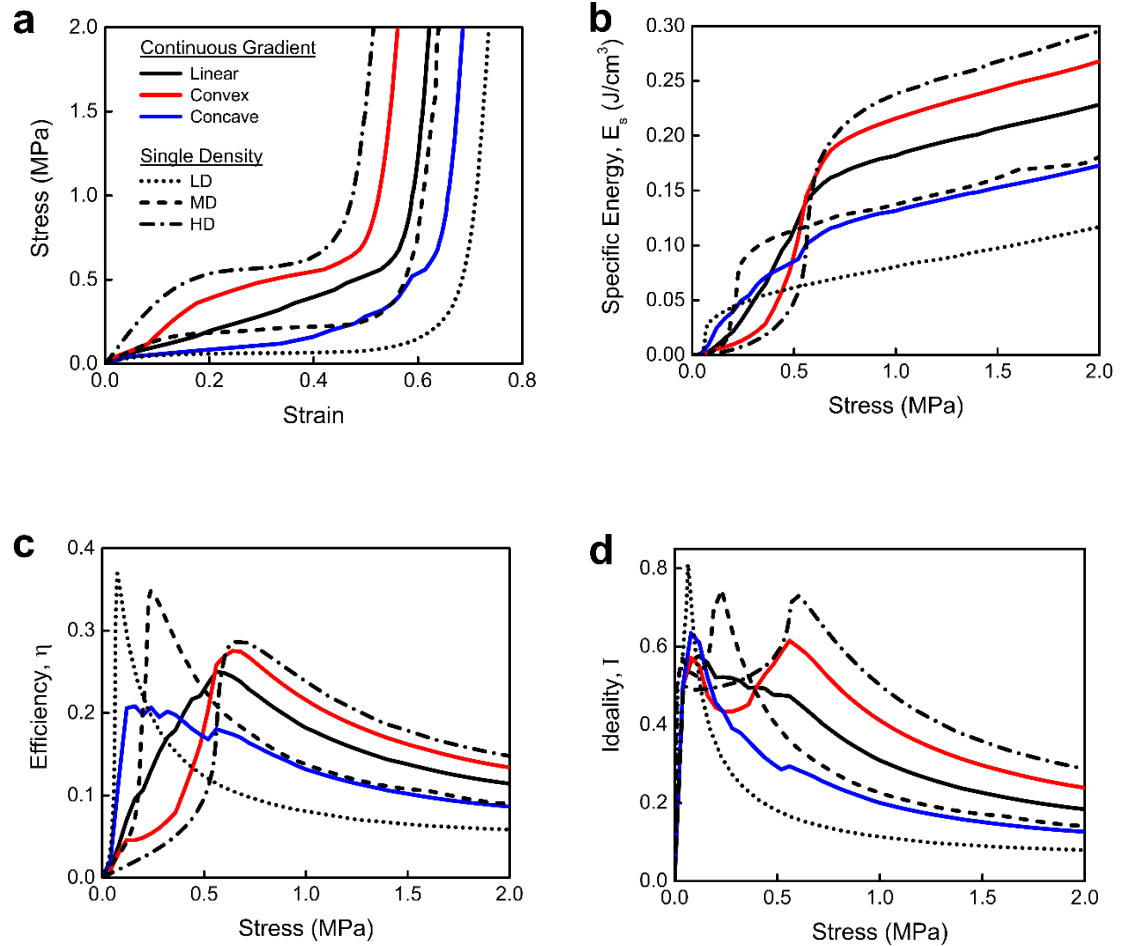
Note. (a)Stress-Strain, (b) Specific Energy-Stress, (c) Efficiency-Stress and (d) Ideality-Stress curves for the three continuously graded structures. Curves of the single-density honeycombs (LD, MD, HD) are shown for comparison.

Considering the load-bearing and energy absorption performances of the three

continuously-graded structures in comparison with the uniform density honeycombs, one

can conclude that there is not a single gradient that offers low density, enhanced load-

34

bearing (strength), and energy absorption capacity at all stress and strain levels. Rather, an optimized structure must be selected based on design criteria and the applications sought. Nevertheless, our findings indicate that density gradation is indeed a promising strategy in achieving structural designs that, when applied in a controlled way, can result in enhanced performance overall.

Chapter 5

Conclusions and Future Directions

5.1 Conclusions

Stress-strain and energy absorption behaviors of density-graded hexagonal honeycombs were studied using an analytical modeling approach. Stress-strain data obtained for single-density honeycomb structures with three different relative densities were used as input to a model that uses an interpolation algorithm to output the stress-strain curve of density-graded structures with known gradients. 28 different cases of 3-stage graded hexagonal honeycombs along with 3 cases of continuously-graded structures were examined. Results confirmed that the modeling approach proposed in this work is capable of predicting the stress-strain and energy absorption behaviors of density-graded honeycombs with good agreement with experimental measurements. It was also found that density gradation can lead to a combination of high strength and improved energy absorption at low structural weights. Density gradation was specifically shown to allow for increasing the densification strain of a graded structure. We also showed that, consistent with previous studies, continuous gradation can lead to an improved energy absorption capacity compared with discretely graded honeycombs. Through the use of a variety of energy absorption metrics, we showed that there is not a single gradient function that leads to the best combination of strength, energy absorption, and low structural weight. Rather, the choice of an optimized gradient depends on the application sought.

5.2 Future Directions

While the approach presented in this work facilitates the study of a complete set of density-graded honeycomb structures with acceptable accuracy and in a computationally efficient manner, there is still a lack of similar models that facilitate the strain rate dependent response of the materials. More advanced models with the capability to address the rate-sensitive response of density-graded structures are being developed by the authors. The modeling approach discussed in this work (in conjunction with its future rate-sensitivity module) has the potential to guide the design of density-graded structure beyond honeycombs fabricated from different materials. One specific area that similar optimization approaches can be applied to is the newly developed areas of functionally graded metamaterials and origami structures [52-55]. Besides, the modeling approach discussed here can supplement advanced finite element models used in the topology optimization of elastoplastic cellular and metamaterials [56, 57].

Recommendations:

- The quasi-static mechanical properties of single-density honeycomb structures have been historically observed to be stronger in the out-of-plane direction as opposed to the in-plane direction (as the cell-walls do not bend but rather compress or extend and thereby resulting in a higher elastic modulus.The plastic collapse strength is also significantly higher due to the involvement of axial and bending deformations). Advancing the concept of this work into investigating the mechanical properties of out-of-plane graded honeycomb structures as they function within a sandwich structure would also be a great next step. These density-graded honeycomb structures in the out-of-plane direction are suitable for

37

use in creating body protective amour, protective headgear and have been found occurring naturally in nature as balsa wood amongst others.

- Investigating the effect of strain/work hardening/softening after a particular graded honeycomb structure has experienced multiple cycles of loading conditions is also a probable future direction.

- Honeycombs which is one of the simplest lattice structures has been employed in this research but the fundamental principle of this work can be extended to even more complex structures that either strut-based or surface-based, e.g. triply periodic minimal surface (gyroids). Auxetic metamaterials with negative poisson's ratio are also a viable candidate for further research due to having better mechanical properties. By carefully engineering the unit cells in these metamaterials, optimized and more favorable mechanical, thermal, etc. properties that do not rely on their chemical composition can be achieved.

- The roles printing imperfections through additive manufacturing have on the cellular structures is a strong future research focus as it affects the material integrity and would showcase itself in the properties of both the single density and density-graded structures.

- The effect on the rate of loading conditions should also be looked into. Cellular materials are strain-rate sensitive and the investigation of the mechanical response of the structure under high speed impact is a viable research area. Efforts are currently underway to include strain rate effects in a computer algorithm that considers the rate-sensitive constitutive response of the honeycombs, as well.

38

References

[1] Habib F, Iovenitti P, Masood S, Nikzad M, Ruan D. Design and evaluation of 3D printed polymeric cellular materials for dynamic energy absorption. International Journal of Advanced Manufacturing Technology 2019; 103: 2347-2361. https://doi.org/10.1007/s00170-019-03541-4

[2] Zhang Q, Yang X, Li P, Huang G, Feng S, Shen C, Han B, Zhang X, Jin F, Xu F, Lu TJ. Bioinspired engineering of honeycomb structure – Using nature to inspire human innovation. Progress in Materials Science 2015; 74: 332-400. https://doi.org/10.1016/j.pmatsci.2015.05.001

[3] Fan H, Luo Y, Yang F, Li W. Approaching perfect energy absorption through structural hierarchy. International Journal of Engineering Sciences 2018; 130: 12-32. https://doi.org/10.1016/j.ijengsci.2018.05.005

[4] Li Z, Liu D, Qian Y, Wang Y, Wang T, Wang L. Enhanced strength and weakened dynamic sensitivity of honeycombs by parallel design. International Journal of Mechanical Sciences 2019; 151: 672-683. https://doi.org/10.1016/j.ijmecsci.2018.12.013

[5] Jardini A, Larosa M, Filho R, de Carvalho Zavaglia CA, Bernards LF, Lambert CS, Calderoni DR, Kharmandayan P. Cranial reconstruction: 3D biomodel and custom-built implant created using additive manufacturing. Journal of Cranio-Maxillofacial Surgery 2014; 42: 1877-1844. https://doi.org/10.1016/j.jcms.2014.07.006

[6] Yan Q, Dong H, Su J, Han J, Song B, Wei Q, Shi Y. A review of 3D printing technology for medical applications. Engineering 2018; 4: 729-742. https://doi.org/10.1016/j.eng.2018.07.021

[7] https://www.globalspec.com/learnmore/materials_chemicals_adhesives/composites_textiles_reinforcements/honeycombs_honeycomb_materials

[8] https://www.wikiwand.com/en/Honeycomb_structure

[9] Gibson L, Ashby M. Cellular solid: Structures and properties, 2n ed. Cambridge: Cambridge University Press; 1997.

[10] Malek S, Gibson L. Effective elastic properties of periodic hexagonal honeycombs. Mechanics of Materials 2015; 91: 226-240. https://doi.org/10.1016/j.mechmat.2015.07.008

[11] Oftadeh R, Haghpanah B, Papadopoulos J, Hamouda AMS, Nayeb-Hashemi H, Vaziri A. Mechanics of anisotropic hierarchical honeycombs. International Journal of Mechanical Sciences 2014; 81: 126-136. https://doi.org/10.1016/j.ijmecsci.2014.02.011

[12] Huang J, Gong X, Zhang Q, Scarpa F, Liu Y, Leng J. In-plane mechanics of a novel zero Poisson's ratio honeycomb core. Composites Part B 2016; 89: 67-76. https://doi.org/10.1016/j.compositesb.2015.11.032

[13] Qiao J, Chen C. In-plane crushing of a hierarchical honeycomb. International Journal of Solids and Structures 2016; 85-86: 57-66. https://doi.org/10.1016/j.ijsolstr.2016.02.003

[14]   Bates SRG, Farrow IR, Trask RS. 3D printed polyurethane honeycombs for repeated tailored energy absorption. Materials and Design 2016; 112: 172-183. https://doi.org/10.1016/j.matdes.2016.08.062

[15]   Kumar S, Ubaid J, Abishera R, Schiffer A, Deshpande VS. Tunable energy absorption characteristics of architected honeycombs enabled via additive manufacturing. ACS Applied Materials and Interfaces 2019; 11: 42549-42560. https://doi.org/10.1021/acsami.9b12880

[16]   Li Z, Jiang Y, Wang T, Wang L, Zhuang W, Liu D. In-plane crushing behaviors of piecewise linear graded honeycombs. Composite Structures 2019; 207: 425-437. https://doi.org/10.1016/j.compstruct.2018.09.036

[17]   Kiernan S, Gilchrist MD. Towards a virtual functionally graded foam: Defining the large strain constitutive response of an isotropic closed cell polymeric cellular solid. International Journal of Engineering Sciences 2010; 48: 1373-1386. https://doi.org/10.1016/j.ijengsci.2010.09.004

[18]   Koohbor B, Kidane A. Design optimization of continuously and discretely graded foam materials for efficient energy absorption. Materials & Design 2016; 102: 151-161. https://doi.org/10.1016/j.matdes.2016.04.031

[19]   Chen D, Kitipornchai S, Yang J. Dynamic response and energy absorption of functionally graded porous structures. Materials & Design 2018; 140: 473-487. https://doi.org/10.1016/j.matdes.2017.12.019

[20]   Duan Y, Zhao X, Du B, Shi X, Zhao H, Hou B, Li Y. Quasi-static compressive behavior and constitutive model of graded foams. International Journal of Mechanical Sciences 2020; 177: 105603. https://doi.org/10.1016/j.ijmecsci.2020.105603

[21]   Liu J, Hou B, Lu F, Zhao H. A theoretical study of shock front propagation in the density graded cellular rods. International Journal of Impact Engineering 2015; 80: 133-142. https://doi.org/10.1016/j.ijimpeng.2015.02.001

[22]   Zheng J, Qin Q, Wang TJ. Impact plastic crushing and design of density-graded cellular materials. Mechanics of Materials 2016; 94: 66-78. https://doi.org/10.1016/j.mechmat.2015.11.014

[23]   Chang B, Zheng Z, Zhang Y, Zhao K, He S, Yu J. Crashworthiness design of graded cellular materials: An asymptotic solution considering loading rate sensitivity. International Journal Impact Engineering 2020; 143: 103611. https://doi.org/10.1016/j.ijimpeng.2020.103611

[24]   Forero Rueda MA, Cui L, Gilchrist MD. Optimisation of energy absorbing liner for equestrian helmets. Part I: Layered foam liner. Materials and Design 2009; 30: 3405-3413. https://doi.org/10.1016/j.matdes.2009.03.037

[25]   Cui L, Forero Rueda MA, Gilchrist MD. Optimisation of energy absorbing liner for equestrian helmets. Part II: Functionally graded foam liner. Materials and Design 2009; 30: 3414-3419. https://doi.org/10.1016/j.matdes.2009.03.044

40

[26]   Gorsse S, Hutchinson C, Gouné M, Banerjee R. Additive manufacturing of metals: a brief review of the characteristic microstructures and properties of steels, Ti-6Al-4V and high-entropy alloys. Science and Technology of Advanced Materials 2017; 18: 584-610. https://doi.org/10.1080/14686996.2017.1361305

[27]   Qi D, Lu Q, He CW, Li Y, Wu W, Xiao D. Impact energy absorption of functionally graded chiral honeycomb structures. Extreme Mechanics Letters 2019; 32: 100568. https://doi.org/10.1016/j.eml.2019.100568

[28]   Qin R, Zhou J, Chen B. Crashworthiness design and multiobjective optimization for hexagon honeycomb structure with functionally graded thickness. Advances in Materials Science and Engineering 2019; https://doi.org/10.1155/2019/8938696

[29]   Yang L, Ferrucci M, Martens R, Dewulf W, Yan C, Shi Y, Yang S. An investigation into the effect of gradients on the manufacturing fidelity of triply periodic minimal surface structures with graded density fabricated by selective laser melting. Journal of Materials Processing Technology 2020; 275: 116367. https://doi.org/10.1016/j.jmatprotec.2019.116367

[30]   Yang L, Martens R, Ferrucci M, Yan C, Shi Y, Yang S. Continuous graded Gyroid cellular structures fabricated by selective laser melting: Design, manufacturing and mechanical properties. Materials and Design 2019; 162: 394-404. https://doi.org/10.1016/j.matdes.2018.12.007

[31]   Mahbod M, Asgari M. Elastic and plastic characterization of a new developed additively manufactured functionally graded porous lattice structure: Analytical and numerical models. International Journal of Mechanical Sciences 2019; 248-266. https://doi.org/10.1016/j.ijmecsci.2019.02.041

[32]   Bandyopadhyay A, Heer B. Additive manufacturing of multi-material structures. Materials Science and Engineering R 2018; 129: 1-16. https://doi.org/10.1016/j.mser.2018.04.001

[33]   Compton BG, Lewis JA. 3D-printing of lightweight cellular composites. Advanced Materials 2014; 26: 5930-5935. https://doi.org/10.1002/adma.201401804

[34]   Li D, Liao W, Dai N, Xie YM. Comparison of mechanical properties and energy absorption of sheet-based and strut-based gyroid cellular structures with graded densities. Materials 2019; 12: 2183. https://doi.org/10.3390/ma12132183

[35]   Yu S, Sun J, Bai J. Investigation of functionally graded TPMS structures fabricated by additive manufacturing. Materials and Design 2019; 182: 108021. https://doi.org/10.1016/j.matdes.2019.108021

[36]   Bates SRG, Farrow I, Stark RS. Compressive behaviour of 3D printed thermoplastic polyurethane honeycombs with graded densities. Materials and Design 2019; 162: 130-142. https://doi.org/10.1016/j.matdes.2018.11.019

41

[37]   Chantarapanich N, Laohaprapanon A, Wisutmethangoon S, Jiamwatthanachai P, Chalermkarnnon P, Suchaitpwatskul S, Puttawibul P, Sitthiseripratip K. Fabrication of three-dimensional honeycomb structure for aeronautical applications using selective laser melting: a preliminary investigation. Rapid Prototyping Journal 2014; 20: 551-558. https://doi.org/10.1108/RPJ-08-2011-0086

[38]   Galehdari SA, Kadkhodayan M, Hadidi-Moud S. Analytical, experimental and numerical study of a graded honeycomb structure under in-plane impact load with low velocity. International Journal of Crashworthiness 2015; 20: 387-400. https://doi.org/10.1080/13588265.2015.1018739

[39]   Zhang X, An L, Ding H. Dynamic crushing behavior and energy absorption of honeycombs with density gradient. Journal of Sandwich Structures & Materials 2103; 16: 125-147. https://doi.org/10.1177/1099636213509099

[40]   Ines Ivañez, Lorena M.Fernandez-Cañadas, SoniaSanchez-Saez. Compressive deformation and energy-absorption capability of aluminium honeycomb core. Composite Structures, 2017, 174. https://doi.org/10.1016/j.compstruct.2017.04.056.

[41]   Mousanzhad D, Ghosh R, Ajdari A. Hamouda AMS, Nayeb-Hashemi H, Vaziri A. Impact resistance and energy absorption of regular and functionally graded hexagonal honeycombs with cell wall material strain hardening. International Journal of Mechanical Sciences 2014; 89: 413-422. https://doi.org/10.1016/j.ijmecsci.2014.10.012

[42]   Mangipudi KR, Van Buuren SW, Onck PR. The microstructural origin of strain hardening in two-dimensional open-cell metal foams. International Journal of Solids and Structures 2010; 47: 2081-2096. https://doi.org/10.1016/j.ijsolstr.2010.04.009

[43]   Avalle M, Belingardi G, Montanini R. Characterization of polymeric structural foams under compressive impact loading by means of energy-absorption diagram. International Journal of Impact Engineering 2001; 25: 455-472. https://doi.org/10.1016/S0734-743X(00)00060-9

[44]   Li QM, Magkiriadis I, Harrigan JJ, Compressive strain at the onset of densification of cellular solids. Journal of Cellular Plastics 2006; 42: 371-392. https://doi.org/10.1177/0021955X06063519

[45]   Technical Specification. NinjaFlex® 3D printing filament, https://ninjatek.com/wp-content/uploads/2019/10/NinjaFlex-TDS.pdf [accessed 26 June 2020].

[46]   Koohbor B, Kidane A, Lu W, Sutton MA. Investigation of the dynamic stress–strain response of compressible polymeric foam using a non-parametric analysis. International Journal of Impact Engineering 2016; 91: 170-182. https://doi.org/10.1016/j.ijimpeng.2016.01.007

[47]   Koohbor B, Singh NK, Kidane A. Radial and axial inertia stresses in high strain rate deformation of polymer foams. International Journal of Mechanical Sciences 2020; 181: 105679. https://doi.org/10.1016/j.ijmecsci.2020.105679

[48] Avalle M, Belingardi G, Montanini R. Characterization of polymeric structural foams under compressive impact loading by means of energy-absorption diagram. International Journal of Impact Engineering 2001; 25: 455-472. https://doi.org/10.1016/S0734-743X(00)00060-9

[49] Li QM, Magkiriadis I, Harrigan JJ, Compressive strain at the onset of densification of cellular solids. Journal of Cellular Plastics 2006; 42: 371-392. https://doi.org/10.1177/0021955X06063519

[50] Maskery I, Hussey A, Panesar A, Aremu A, Tuck C, Ashcroft I, Hague R. An investigation into reinforced and functionally graded lattice structures. Journal of Cellular Plastics 2016; 53: 151-165. https://doi.org/10.1177/0021955X16639035

[51] Bai L, Gong C, Chen X, Sun Y, Xin L, Pu H, Peng Y, Luo J. Mechanical properties and energy absorption capabilities of functionally graded lattice structures: Experimental and simulations. International Journal of Mechanical Sciences 2020; 182: 105735. https://doi.org/10.1016/j.ijmecsci.2020.105735

[52] Ma J, Song J, Chen Y. An origami-inspired structure with graded stiffness. International Journal of Mechanical Sciences 2018; 136: 134-142. https://doi.org/10.1016/j.ijmecsci.2017.12.026

[53] Li Z, Chen W, Hao H. Functionally graded truncated square pyramid folded structures with foam filler under dynamic crushing. Composites Part B 2019; 177: 107410. https://doi.org/10.1016/j.compositesb.2019.107410

[54] Yuan L, Dai H, Song J, Ma J, Chen Y. The behavior of a functionally gradedorigami structure subjected to quasi-static compression. Materials and Design 2020; 189: 108494. https://doi.org/10.1016/j.matdes.2020.108494

[55] Wang Y, Sigmund O. Quasiperiodic mechanical metamaterials with extreme isotropic stiffness. Extreme Mechanics Letters 2020; 34: 100596. https://doi.org/10.1016/j.eml.2019.100596

[56] Panesar A, Abdi M, Hickman D, Ashcroft I. Strategies for functionally graded lattice structures derived using topology optimisation for Additive Manufacturing. Additive Manufacturing 2018; 19: 81-94. https://doi.org/10.1016/j.addma.2017.11.008

[57] Rohanifar M, Hatami-Marbini H. Numerical modelling of mechanical properties of 2D cellular solids with bi-modulus cell walls. Mechanics of Advanced Materials and Structures 2019 (in press) https://doi.org/10.1080/15376494.2018.1563251

43

Comparison of 2-stage diagrams from both Analytical Model and Experiment

Figure A1

Stress-Strain Diagrams
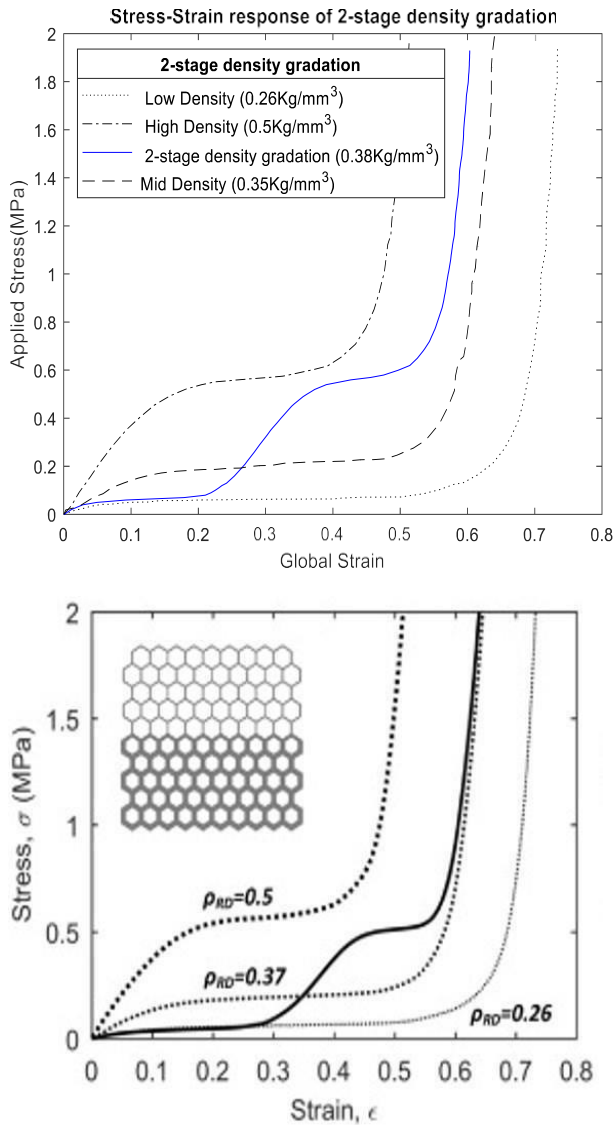
Note: Stress-Strain diagrams of 2-stage Graded Hexagonal Honeycomb obtained from Model and Experiment Respectively.

Figure A2

Stress-Specific Energy Diagrams
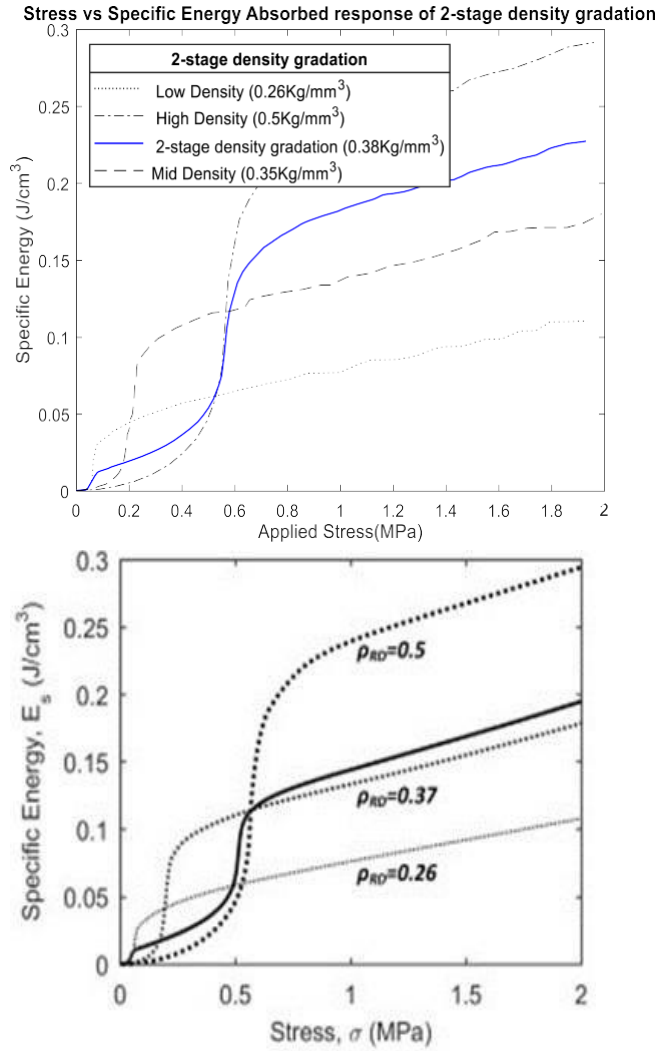
Note: Stress-Specific Energy diagrams of 2-stage graded hexagonal honeycomb obtained from model and experiment respectively.

MATLAB Code

The MATLAB code used for the virtual experiments can be found below.

clear;

```matlab
clc;

input=xlsread('...xlsx');                    % input data

density=input(:,1);

 stress=input(:,2);

strain=input(:,3);

H=65.5;                                       % total thickness in mm

dist=xlsread('...xlsx');                      % density gradation

thickness_dist=dist(:,1);                     % thickness in every 0.1mm

density_dist1=dist(:,2);                       % density distribution of the gradation distribution

pressure=0:0.01:2

h_0=H/(length(thickness_dist)-1);

for i=1:length(pressure)                      % pressure for loop

 stress_applied(i)=pressure(i);               % stress in MPa

 output(i,2)=stress_applied(i);               % stress as an output in MPa

 Final_thickness1(i)=0;                       % incorporating the final thickness
in the for loop

for j=1:length(thickness_dist)                % density distribution for loop

 local_strain1(j)=griddata(density,stress,strain,density_dist1(j),stress_applied(i));
        % linear interpolation to derive local strain
```

46

```
h_f1(j)=h_0*exp((-1)*(local_strain1(j)));
```

```
Final_thickness1(i)=Final_thickness1(i)+h_f1(j);    % final thickness of the graded
```

```
global_strain1(i)=log(H/Final_thickness1(i));       % global strain of the graded
```

```
end  output(i,3)=global_strain1(i);                 % global strain as an output
```

Overview of the Input and Output Files from the Virtual Experiments

The following tables are the data input for the 3-Stage Density Gradation

Virtual Experiments

Table A1

Data Input for Density Gradation

Density(Kg/mm^3)	Stress(Mpa)	Strain
0.26	0	0
0.26	0.01716714	0.015905
0.26	0.02543806	0.029161
0.26	0.03390794	0.039769
0.26	0.041927	0.055674
0.26	0.04232097	0.069329
0.26	0.04835914	0.087752
0.26	0.05127885	0.10617
0.26	0.05147642	0.124584
0.26	0.05761223	0.143006
0.26	0.05771099	0.161425
0.26	0.05781119	0.17677
0.26	0.05982393	0.198262
0.26	0.06066362	0.211986
0.26	0.06082827	0.230529
0.26	0.061882	0.255029

47

Density(Kg/mm^3)	Stress(Mpa)	Strain
0.26	0.06311684	0.274984
0.26	0.06324855	0.294929
0.26	0.06361077	0.315648
0.26	0.06377542	0.330737
0.26	0.06398397	0.350174
0.26	0.06414587	0.365519
0.26	0.06458218	0.399278
0.26	0.06789154	0.411554
0.26	0.07210646	0.445326
0.26	0.07227934	0.466809
0.26	0.07246868	0.484455
0.26	0.07269918	0.500567
0.26	0.08665286	0.535113
0.26	0.10380065	0.558921
0.26	0.12594543	0.580433
0.26	0.13078599	0.592716
0.26	0.16370405	0.614243
0.26	0.2123512	0.637325
0.26	0.27233473	0.654284
0.26	0.32641737	0.665097
0.26	0.39342794	0.675928
0.26	0.47787444	0.683712
0.26	0.56730969	0.689969
0.26	0.63189999	0.694658
0.26	0.71968878	0.699889
0.26	0.81328955	0.704105
0.26	0.87651882	0.708434
0.26	0.93506111	0.708594
0.26	0.99668879	0.70887
0.26	1.06180495	0.713641
0.26	1.11677349	0.7167
0.26	1.1682749	0.716768
0.26	1.21092955	0.716893
0.26	1.26269416	0.717931
0.26	1.30558358	0.719599
0.26	1.35705657	0.722316
0.26	1.40230759	0.723299
0.26	1.461975	0.723378
0.26	1.55144317	0.726566
0.26	1.61111058	0.726645
0.26	1.68068962	0.729806

Density(Kg/mm^3)	Stress(Mpa)	Strain
0.26	1.74035702	0.729885
0.26	1.7947049	0.733125
0.26	1.86960347	0.733214
0.26	1.9367293	0.733492
0.33	0	0
0.33	0.01843318	0.002827
0.33	0.0322726	0.022075
0.33	0.06990954	0.043432
0.33	0.08616598	0.058381
0.33	0.11060738	0.07089
0.33	0.13050193	0.089196
0.33	0.15039648	0.110044
0.33	0.16283057	0.127333
0.33	0.17194891	0.144622
0.33	0.17899489	0.166996
0.33	0.18272512	0.185302
0.33	0.18620667	0.207675
0.33	0.18686982	0.224964
0.33	0.19184346	0.245101
0.33	0.1926724	0.262898
0.33	0.19815668	0.274205
0.33	0.20276498	0.29056
0.33	0.20344861	0.308866
0.33	0.21256694	0.327172
0.33	0.21505376	0.345477
0.33	0.21754058	0.363783
0.33	0.21919846	0.382089
0.33	0.22001817	0.401581
0.33	0.22168528	0.420226
0.33	0.22701503	0.440057
0.33	0.22748786	0.459889
0.33	0.23121808	0.478194
0.33	0.24655347	0.495483
0.33	0.27639529	0.519891
0.33	0.30830946	0.537688
0.33	0.37794038	0.558282
0.33	0.45005812	0.571249
0.33	0.51430094	0.580402
0.33	0.57439905	0.581927
0.33	0.63781293	0.586504
0.33	0.65646407	0.594131

49

Density(Kg/mm^3)	Stress(Mpa)	Strain
0.33	0.70744385	0.5975
0.33	0.78370629	0.600914
0.33	0.8594161	0.603284
0.33	0.92628389	0.606335
0.33	0.96109935	0.606335
0.33	1.02547242	0.611565
0.33	1.11403869	0.613962
0.33	1.18590775	0.617929
0.33	1.26608278	0.619759
0.33	1.35700087	0.62281
0.33	1.44492373	0.626166
0.33	1.54011362	0.630519
0.33	1.582804	0.63357
0.33	1.64248765	0.633794
0.33	1.70714493	0.635095
0.33	1.7734601	0.635319
0.33	1.85801193	0.635319
0.33	1.91990608	0.636845
0.33	1.98898438	0.639896
0.5	0	0
0.5	0.03748287	0.01136
0.5	0.08991019	0.022202
0.5	0.155671	0.039075
0.5	0.21914444	0.05442
0.5	0.28719262	0.072822
0.5	0.35274047	0.093051
0.5	0.4036552	0.112649
0.5	0.45433914	0.134077
0.5	0.4924323	0.157014
0.5	0.52171724	0.181463
0.5	0.53963662	0.20437
0.5	0.55163039	0.22371
0.5	0.55650899	0.245582
0.5	0.56399248	0.274577
0.5	0.56846267	0.297465
0.5	0.57508776	0.324933
0.5	0.58838398	0.347835
0.5	0.60379945	0.372264
0.5	0.61747437	0.391606
0.5	0.65427696	0.411998
0.5	0.70874349	0.433432

50

Density(Kg/mm^3)	Stress(Mpa)	Strain
0.5	0.77574734	0.448781
0.5	0.85308263	0.461094
0.5	0.92518091	0.468824
0.5	1.0135303	0.476576
0.5	1.12285839	0.481307
0.5	1.16325941	0.485941
0.5	1.23220431	0.487563
0.5	1.32808321	0.492275
0.5	1.42812935	0.493942
0.5	1.48618242	0.498601
0.5	1.58092274	0.501786
0.5	1.65266955	0.503413
0.5	1.75526117	0.507117
0.5	1.85953988	0.511332
0.5	1.96042659	0.513

DISTRIBUTION

Below is the Gradation Distribution of Case 2 (1-2-6)

Table A2

Gradation Distribution of Case 2 (1-2-6)

H	Gradation	H	Gradation	H	Gradation	H	Gradation
0	0.26	4.1	0.26	8.2	0.35	12.3	0.35
0.1	0.26	4.2	0.26	8.3	0.35	12.4	0.35
0.2	0.26	4.3	0.26	8.4	0.35	12.5	0.35
0.3	0.26	4.4	0.26	8.5	0.35	12.6	0.35
0.4	0.26	4.5	0.26	8.6	0.35	12.7	0.35
0.5	0.26	4.6	0.26	8.7	0.35	12.8	0.35
0.6	0.26	4.7	0.26	8.8	0.35	12.9	0.35
0.7	0.26	4.8	0.26	8.9	0.35	13	0.35
0.8	0.26	4.9	0.26	9	0.35	13.1	0.35
0.9	0.26	5	0.26	9.1	0.35	13.2	0.35

51

H	Gradation	H	Gradation	H	Gradation	H	Gradation
1	0.26	5.1	0.26	9.2	0.35	13.3	0.35
1.1	0.26	5.2	0.26	9.3	0.35	13.4	0.35
1.2	0.26	5.3	0.26	9.4	0.35	13.5	0.35
1.3	0.26	5.4	0.26	9.5	0.35	13.6	0.35
1.4	0.26	5.5	0.26	9.6	0.35	13.7	0.35
1.5	0.26	5.6	0.26	9.7	0.35	13.8	0.35
1.6	0.26	5.7	0.26	9.8	0.35	13.9	0.35
1.7	0.26	5.8	0.26	9.9	0.35	14	0.35
1.8	0.26	5.9	0.26	10	0.35	14.1	0.35
1.9	0.26	6	0.26	10.1	0.35	14.2	0.35
2	0.26	6.1	0.26	10.2	0.35	14.3	0.35
2.1	0.26	6.2	0.26	10.3	0.35	14.4	0.35
2.2	0.26	6.3	0.26	10.4	0.35	14.5	0.35
2.3	0.26	6.4	0.26	10.5	0.35	14.6	0.35
2.4	0.26	6.5	0.26	10.6	0.35	14.7	0.35
2.5	0.26	6.6	0.26	10.7	0.35	14.8	0.35
2.6	0.26	6.7	0.26	10.8	0.35	14.9	0.35
2.7	0.26	6.8	0.26	10.9	0.35	15	0.35
2.8	0.26	6.9	0.26	11	0.35	15.1	0.35
2.9	0.26	7	0.26	11.1	0.35	15.2	0.35
3	0.26	7.1	0.26	11.2	0.35	15.3	0.35
3.1	0.26	7.2	0.26	11.3	0.35	15.4	0.35
3.2	0.26	7.3	0.26	11.4	0.35	15.5	0.35
3.3	0.26	7.4	0.35	11.5	0.35	15.6	0.35
3.4	0.26	7.5	0.35	11.6	0.35	15.7	0.35
3.5	0.26	7.6	0.35	11.7	0.35	15.8	0.35
3.6	0.26	7.7	0.35	11.8	0.35	15.9	0.35
3.7	0.26	7.8	0.35	11.9	0.35	16	0.35
3.8	0.26	7.9	0.35	12	0.35	16.1	0.35
3.9	0.26	8	0.35	12.1	0.35	16.2	0.35
4	0.26	8.1	0.35	12.2	0.35	16.3	0.35
16.4	0.35	20.5	0.35	24.6	0.5	28.7	0.5
16.5	0.35	20.6	0.35	24.7	0.5	28.8	0.5
16.6	0.35	20.7	0.35	24.8	0.5	28.9	0.5
16.7	0.35	20.8	0.35	24.9	0.5	29	0.5
16.8	0.35	20.9	0.35	25	0.5	29.1	0.5
16.9	0.35	21	0.35	25.1	0.5	29.2	0.5
17	0.35	21.1	0.35	25.2	0.5	29.3	0.5
17.1	0.35	21.2	0.35	25.3	0.5	29.4	0.5
17.2	0.35	21.3	0.35	25.4	0.5	29.5	0.5
17.3	0.35	21.4	0.35	25.5	0.5	29.6	0.5

H	Gradation	H	Gradation	H	Gradation	H	Gradation
17.4	0.35	21.5	0.35	25.6	0.5	29.7	0.5
17.5	0.35	21.6	0.35	25.7	0.5	29.8	0.5
17.6	0.35	21.7	0.35	25.8	0.5	29.9	0.5
17.7	0.35	21.8	0.35	25.9	0.5	30	0.5
17.8	0.35	21.9	0.5	26	0.5	30.1	0.5
17.9	0.35	22	0.5	26.1	0.5	30.2	0.5
18	0.35	22.1	0.5	26.2	0.5	30.3	0.5
18.1	0.35	22.2	0.5	26.3	0.5	30.4	0.5
18.2	0.35	22.3	0.5	26.4	0.5	30.5	0.5
18.3	0.35	22.4	0.5	26.5	0.5	30.6	0.5
18.4	0.35	22.5	0.5	26.6	0.5	30.7	0.5
18.5	0.35	22.6	0.5	26.7	0.5	30.8	0.5
18.6	0.35	22.7	0.5	26.8	0.5	30.9	0.5
18.7	0.35	22.8	0.5	26.9	0.5	31	0.5
18.8	0.35	22.9	0.5	27	0.5	31.1	0.5
18.9	0.35	23	0.5	27.1	0.5	31.2	0.5
19	0.35	23.1	0.5	27.2	0.5	31.3	0.5
19.1	0.35	23.2	0.5	27.3	0.5	31.4	0.5
19.2	0.35	23.3	0.5	27.4	0.5	31.5	0.5
19.3	0.35	23.4	0.5	27.5	0.5	31.6	0.5
19.4	0.35	23.5	0.5	27.6	0.5	31.7	0.5
19.5	0.35	23.6	0.5	27.7	0.5	31.8	0.5
19.6	0.35	23.7	0.5	27.8	0.5	31.9	0.5
19.7	0.35	23.8	0.5	27.9	0.5	32	0.5
19.8	0.35	23.9	0.5	28	0.5	32.1	0.5
19.9	0.35	24	0.5	28.1	0.5	32.2	0.5
20	0.35	24.1	0.5	28.2	0.5	32.3	0.5
20.1	0.35	24.2	0.5	28.3	0.5	32.4	0.5
20.2	0.35	24.3	0.5	28.4	0.5	32.5	0.5
20.3	0.35	24.4	0.5	28.5	0.5	32.6	0.5
20.4	0.35	24.5	0.5	28.6	0.5	32.7	0.5
32.8	0.5	36.9	0.5	41	0.5	45.1	0.5
32.9	0.5	37	0.5	41.1	0.5	45.2	0.5
33	0.5	37.1	0.5	41.2	0.5	45.3	0.5
33.1	0.5	37.2	0.5	41.3	0.5	45.4	0.5
33.2	0.5	37.3	0.5	41.4	0.5	45.5	0.5
33.3	0.5	37.4	0.5	41.5	0.5	45.6	0.5
33.4	0.5	37.5	0.5	41.6	0.5	45.7	0.5
33.5	0.5	37.6	0.5	41.7	0.5	45.8	0.5
33.6	0.5	37.7	0.5	41.8	0.5	45.9	0.5
33.7	0.5	37.8	0.5	41.9	0.5	46	0.5

H	Gradation	H	Gradation	H	Gradation	H	Gradation
33.8	0.5	37.9	0.5	42	0.5	46.1	0.5
33.9	0.5	38	0.5	42.1	0.5	46.2	0.5
34	0.5	38.1	0.5	42.2	0.5	46.3	0.5
34.1	0.5	38.2	0.5	42.3	0.5	46.4	0.5
34.2	0.5	38.3	0.5	42.4	0.5	46.5	0.5
34.3	0.5	38.4	0.5	42.5	0.5	46.6	0.5
34.4	0.5	38.5	0.5	42.6	0.5	46.7	0.5
34.5	0.5	38.6	0.5	42.7	0.5	46.8	0.5
34.6	0.5	38.7	0.5	42.8	0.5	46.9	0.5
34.7	0.5	38.8	0.5	42.9	0.5	47	0.5
34.8	0.5	38.9	0.5	43	0.5	47.1	0.5
34.9	0.5	39	0.5	43.1	0.5	47.2	0.5
35	0.5	39.1	0.5	43.2	0.5	47.3	0.5
35.1	0.5	39.2	0.5	43.3	0.5	47.4	0.5
35.2	0.5	39.3	0.5	43.4	0.5	47.5	0.5
35.3	0.5	39.4	0.5	43.5	0.5	47.6	0.5
35.4	0.5	39.5	0.5	43.6	0.5	47.7	0.5
35.5	0.5	39.6	0.5	43.7	0.5	47.8	0.5
35.6	0.5	39.7	0.5	43.8	0.5	47.9	0.5
35.7	0.5	39.8	0.5	43.9	0.5	48	0.5
35.8	0.5	39.9	0.5	44	0.5	48.1	0.5
35.9	0.5	40	0.5	44.1	0.5	48.2	0.5
36	0.5	40.1	0.5	44.2	0.5	48.3	0.5
36.1	0.5	40.2	0.5	44.3	0.5	48.4	0.5
36.2	0.5	40.3	0.5	44.4	0.5	48.5	0.5
36.3	0.5	40.4	0.5	44.5	0.5	48.6	0.5
36.4	0.5	40.5	0.5	44.6	0.5	48.7	0.5
36.5	0.5	40.6	0.5	44.7	0.5	48.8	0.5
36.6	0.5	40.7	0.5	44.8	0.5	48.9	0.5
36.7	0.5	40.8	0.5	44.9	0.5	49	0.5
36.8	0.5	40.9	0.5	45	0.5	49.1	0.5
49.2	0.5	53.3	0.5	57.4	0.5	61.5	0.5
49.3	0.5	53.4	0.5	57.5	0.5	61.6	0.5
49.4	0.5	53.5	0.5	57.6	0.5	61.7	0.5
49.5	0.5	53.6	0.5	57.7	0.5	61.8	0.5
49.6	0.5	53.7	0.5	57.8	0.5	61.9	0.5
49.7	0.5	53.8	0.5	57.9	0.5	62	0.5
49.8	0.5	53.9	0.5	58	0.5	62.1	0.5
49.9	0.5	54	0.5	58.1	0.5	62.2	0.5
50	0.5	54.1	0.5	58.2	0.5	62.3	0.5

H	Gradation	H	Gradation	H	Gradation	H	Gradation
50.1	0.5	54.2	0.5	58.3	0.5	62.4	0.5
50.2	0.5	54.3	0.5	58.4	0.5	62.5	0.5
50.3	0.5	54.4	0.5	58.5	0.5	62.6	0.5
50.4	0.5	54.5	0.5	58.6	0.5	62.7	0.5
50.5	0.5	54.6	0.5	58.7	0.5	62.8	0.5
50.6	0.5	54.7	0.5	58.8	0.5	62.9	0.5
50.7	0.5	54.8	0.5	58.9	0.5	63	0.5
50.8	0.5	54.9	0.5	59	0.5	63.1	0.5
50.9	0.5	55	0.5	59.1	0.5	63.2	0.5
51	0.5	55.1	0.5	59.2	0.5	63.3	0.5
51.1	0.5	55.2	0.5	59.3	0.5	63.4	0.5
51.2	0.5	55.3	0.5	59.4	0.5	63.5	0.5
51.3	0.5	55.4	0.5	59.5	0.5	63.6	0.5
51.4	0.5	55.5	0.5	59.6	0.5	63.7	0.5
51.5	0.5	55.6	0.5	59.7	0.5	63.8	0.5
51.6	0.5	55.7	0.5	59.8	0.5	63.9	0.5
51.7	0.5	55.8	0.5	59.9	0.5	64	0.5
51.8	0.5	55.9	0.5	60	0.5	64.1	0.5
51.9	0.5	56	0.5	60.1	0.5	64.2	0.5
52	0.5	56.1	0.5	60.2	0.5	64.3	0.5
52.1	0.5	56.2	0.5	60.3	0.5	64.4	0.5
52.2	0.5	56.3	0.5	60.4	0.5	64.5	0.5
52.3	0.5	56.4	0.5	60.5	0.5	64.6	0.5
52.4	0.5	56.5	0.5	60.6	0.5	64.7	0.5
52.5	0.5	56.6	0.5	60.7	0.5	64.8	0.5
52.6	0.5	56.7	0.5	60.8	0.5	64.9	0.5
52.7	0.5	56.8	0.5	60.9	0.5	65	0.5
52.8	0.5	56.9	0.5	61	0.5	65.1	0.5
52.9	0.5	57	0.5	61.1	0.5	65.2	0.5
53	0.5	57.1	0.5	61.2	0.5	65.3	0.5
53.1	0.5	57.2	0.5	61.3	0.5	65.4	0.5
53.2	0.5	57.3	0.5	61.4	0.5	65.5	0.5

DISTRIBUTION OUTPUT

The tables below are the Global Stress-Strain Output for Case 2 (1-2-6)

Table A3

Global Stress-Strain Output for Case 2 (1-2-6)

Stress	Strain
0	-0.00153
0.01	0.001875
0.02	0.005915
0.03	0.012611
0.04	0.018004
0.05	0.025598
0.06	0.038608
0.07	0.061054
0.08	0.071356
0.09	0.076045
0.1	0.079984
0.11	0.083735
0.12	0.088229
0.13	0.093205
0.14	0.097886
0.15	0.102468
0.16	0.107711
0.17	0.113607
0.18	0.122273
0.19	0.137855
0.2	0.148456
.	.
.	.
.	.
1.93	0.560473

56